J|A|C|S
ARTICLES
Published on Web 01/26/2006

Large Area Liquid Crystal Monodomain Field-Effect Transistors

Albert J. J. M. van Breemen,*,† Peter T. Herwig,† Ceciel H. T. Chlon,† Jörgen Sweelssen,† Herman F. M. Schoo,† Sepas Setayesh,‡ Willie M. Hardeman,‡ Christian A. Martin,‡ Dago M. de Leeuw,‡ Josué J. P. Valeton,§ Cees W. M. Bastiaansen,§ Dirk J. Broer,§,‡ Andreea R. Popa-Merticaru,|| and Stefan C. J. Meskers||

Contribution from TNO Science and Industry, De Rondom 1, P. O. Box 6235, 5600 HE Eindhoven, The Netherlands, Philips Research Laboratories, Professor Holstlaan 4, 5656 AA, Eindhoven, The Netherlands, Department of Polymer Technology, Faculty of Chemistry and Chemical Engineering, Eindhoven University of Technology, P. O Box 513, 5600 MB Eindhoven, The Netherlands, and Laboratory of Macromolecular and Organic Chemistry, Eindhoven University of Technology, P.O. Box 513, 5600 MB Eindhoven, The Netherlands

Received August 29, 2005; E-mail: albert.vanbreemen@tno.nl

Abstract: Butyl, hexyl, and decyl derivatives of the liquid-crystalline organic semiconductor 5,5″-bis(5-alkyl-2-thienylethynyl)-2,2′:5′,2″-terthiophene were synthesized and studied with respect to their structural, optical, and electrical properties. By means of an optimized thermal annealing scheme the hexyl and decyl compounds could be processed into self-assembled monodomain films of up to 150 mm in diameter. These were investigated with X-ray diffractometry, which revealed a clearly single-crystalline monoclinic morphology with lamellae parallel to the substrate. Within the lamellae the molecules were found to arrange with a tilt of about 50° with the rubbing direction of the polyimide alignment layer. The resulting, close side-to-side packing was confirmed by measurements of the UV/vis absorption, which showed a dichroic ratio of 19 and indicated H-aggregation. AFM analyses revealed self-affinity in the surface roughness of the monodomain. The compounds showed bipolar charge transport in TOF measurements, with hole mobilities reaching up to 0.02 cm^2/Vs and maximum electron mobilities around 0.002 cm^2/Vs. The hexyl derivative was processed into large-area monodomain top-gate field-effect transistors, which were stable for months and showed anisotropic hole mobilities of up to 0.02 cm^2/Vs. Compared to multidomain bottom-gate transistors the monodomain formation allowed for a mobility increase by 1 order of magnitude.

1. Introduction

Over the last years the field of organic electronics has seen enormous progress. The performance of the best organic field-effect transistors (OFETs) is already exceeding that of amorphous silicon devices, and the first integrated organic circuits such as drivers for low-end displays and low-cost memory devices for disposable smart labels and transponders have been demonstrated.[1,2]

However, organic electronics are still far from exploiting their market potential. The key to their commercial success is the availability of a high-mobility organic semiconductor that is solution-processable and stable under standard environmental conditions. OFETs from single crystals of small conjugated molecules, such as oligoacene and thiophene derivatives, exhibit mobilities of up to 15 cm^2/Vs, but their production relies on technologically unfavorable vapor growth routes.[3−6] Semiconducting polymers, in contrast, are typically solution processable but exhibit instabilities under the influence of water and oxygen. Even though the deposition of tetrathiafulvalene derivatives (TTF) in single crystals and modified doctor blading of functionalized anthradithiophenes have recently yielded solution-processed OFETs with promising mobilities in the order of 1 cm^2/Vs, the suitability of these processes for large-area deposition has not been demonstrated.[7−9]

† TNO Science and Industry.
‡ Philips Research Laboratories.
§ Faculty of Chemistry and Chemical Engineering, Eindhoven University of Technology.
|| Laboratory of Macromolecular and Organic Chemistry, Eindhoven University of Technology.

(1) Huitema, H. E. A.; Gelinck, G. H.; van der Putten, J. B. P. H.; Kuijk, K. E.; Hart, C. M.; Cantatore, E.; Herwig, P. T.; van Breemen, A. J. J. M.; de Leeuw, D. M. *Nature* **2001**, *414*, 599.
(2) Gelinck, G. H.; et al. *Nat. Mater.* **2004**, *3*, 106.
(3) Lin, Y.-Y.; Gundlach, D. J.; Nelson, S. F.; Jackson, T. N. *IEEE Trans. Electron Devices* **1997**, *44*, 1325.
(4) Sundar, V. C.; Zaumseil, J.; Podzorov, V.; Menard, E.; Willett, R. L.; Someya, T.; Gershenson, M. E.; Rogers, J. A. *Science* **2004**, *303*, 1644.
(5) Meng, H.; Sun, F.; Goldfinger, M. B.; Jaycox, G. D.; Li, A.; Marshall, W. J.; Blackman, G. S. *J. Am. Chem. Soc.* **2005**, *127*, 2406.
(6) Mello, J. A.; Newman, C. R.; Gerlach, C. P.; Kelley, T. W.; Muyres, D. V.; Fritz, S. E.; Toney, M. F.; Frisbie, C. D. *J. Am. Chem. Soc.* **2005**, *127*, 3997.
(7) Mas-Torrent, M.; Hadley, P.; Bromley, S. T.; Ribas, X.; Tarrés, J.; Mas, M.; Molins, E.; Veciana, J.; Rovira, C. *J. Am. Chem. Soc.* **2004**, *126*, 8546.
(8) Mas-Torrent, M.; Hadley, P.; Bromley, S. T.; Crivillers, N.; Veciana, J.; Rovira, C. *Appl. Phys. Lett.* **2005**, *86*, 012220.
(9) Payne, M. M.; Parkin, S. R.; Anthony, J. E.; Kuo, C.-C.; Jackson, T. N. *J. Am. Chem. Soc.* **2005**, *127*, 4986.

10.1021/ja055337l CCC: $33.50

In this paper, we report on a successful route toward large-area semiconducting films with a highly ordered morphology—the controlled self-organization of solution-processable liquid-crystalline organic semiconductors. The potential of liquid crystals (LCs) in organic electronics has only recently been recognized.[10] The first report of a time-of-flight (TOF) mobility of 0.1 cm^2/Vs in discotic liquid crystals was published in 1994.[11] Since then, numerous systematic studies have been carried out. In a calamitic dioctylterthiophene (8-TTP-8), Funahashi and Hanna achieved ambipolar TOF mobilities of 0.01 cm^2/Vs.[12] In general, highest mobilities can only be expected for ordered monodomains with a large orbital overlap of neighboring molecules. In optoelectronics, the alignment of LCs is often achieved with the help of rubbed layers of polyimide (PI) or modified poly(phenylenevinylene) (PPV)[10]. This concept has also been applied in the production of the first LC polymer thin-film transistor (TFT) in 2000.[13] A thin film of poly-9,9-dioctyl-fluorene-*alt*-bithiophene (F8T2) was deposited on a layer of rubbed PI. A glass formed from the nematic phase then exhibited mobilities of up to 0.02 cm^2/Vs. Recently, quenching of another LC oligofluorene semiconductor in the nematic phase allowed for the fabrication of top-gate transistors with mobilities on the order of 0.01 cm^2/Vs.[14] However, alignment processes that can be carried out in thermal quasi-equilibrium and that lead to large monodomains have not yet been demonstrated for LC organic semiconductors.

The processability of LC semiconductors into large-area ordered films depends strongly on their liquid-crystalline mesophases. In general, a direct transition from the isotropic to a highly ordered smectic or crystalline phase results in non-aligned multidomain structures, even in the presence of alignment layers.[15] Hence, our synthesis aimed at an organic liquid-crystalline semiconductor with a tailored, more diversified phase behavior. The formation of an aligned, defect-free monodomain was expected to be facilitated when a sequence of phases with increasing order and small formation enthalpies is present upon cooling from the isotropic phase. A typical sequence of phases which might enable the formation of monolithic structures could be: from the isotropic phase to the nematic phase and then to low ordered and highly ordered smectic phases and finally to a crystalline phase. Here, the gradual increase in order and the slow transitions between the phases were expected to suppress the formation of a multidomain structure while going through a phase transition.

Liquid-crystalline semiconductors with the above-mentioned phase behavior are rare. A nice example, 5,5″-bis(5-butyl-2-thienylethynyl)-2,2′:5′,2″-terthiophene (**6a** in Scheme 1), was published by Ikeda.[16] This material, developed to enhance the optical-field-induced reorientation of LCs, shows upon cooling from the isotropic phase a broad nematic phase, a smectic B phase, and a crystalline phase. Since a nematic phase is preferred for alignment, the corresponding transition temperature is important if plastic substrates such as poly(ethylene tereftalate) are considered. The transition to the nematic phase for **6a** is at a relatively low temperature of 101 °C, making this class of materials potentially very interesting for self-organized monodomain FETs.

Scheme 1. Synthesis of Liquid-Crystalline Semiconductors **6**

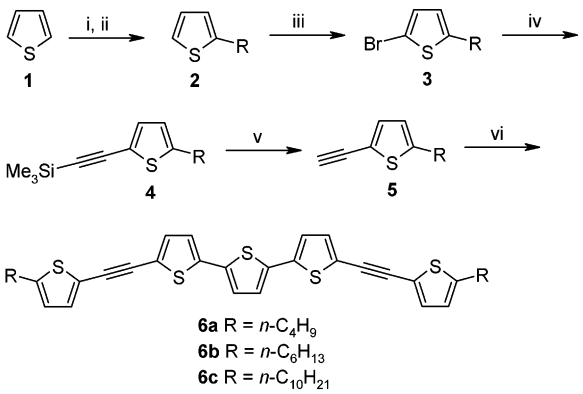

6a R = *n*-C_4H_9
6b R = *n*-C_6H_{13}
6c R = *n*-$C_{10}H_{21}$

i: BuLi
ii: $Br(CH_2)_nCH_3$
iii: NBS, THF
iv: trimethylsilylacetylene, $Pd(PPh_3)_4$, CuI, diisopropylamine
v: TBAF/silica, THF
vi: dibromoterthiophene, $Pd(PPh_3)_4$, CuI, diisopropylamine, THF

In this work, we report on the design and characterization of soluble liquid-crystalline semiconductors (Scheme 1). By means of optimized thermal processing, these semiconductors self-organize in monodomain thin films over large areas of up to 150 mm in diameter, which can be used as active layers in field-effect transistors. The formation of monodomains is accompanied by a 10-fold improvement of the charge carrier mobility if compared to devices based on multidomain thin films.

2. Experimental Section

General. All reagents and chemicals were obtained from commercial sources and used without further purification. All reactions were performed under an inert atmosphere of nitrogen. ^{1}H NMR spectra were recorded on a Varian 400 MHz spectrometer in deuterated chloroform with tetramethylsilane as an internal reference. The ^{13}C NMR spectra were recorded at 100 MHz on the same spectrometer in deuterated chloroform. Chemical shifts were defined relative to the ^{13}C resonance shift of chloroform (77.0 ppm). The absorption of the organic semiconductors in solution and in thin films was determined with a Perkin-Elmer Lambda 950 UV/vis spectrometer. The phase transition temperatures were determined with a TA Instruments Q1000 differential scanning calorimeter (DSC). The heating and cooling rates were kept constant at 10 °C/min. The reported temperatures are the onset temperatures. A Veeco multimode scanning probe microscope was used to investigate the surface structure of organic semiconductor films. For the measurements a stiff cantilever was used (40 N/m, 325 kHz). All images were recorded with a *Q*-factor of 1000 and a scanning resolution of 512 pixels × 512 pixels. Fourier analysis was carried out ex situ with image analysis software from Nanoscope. TOF mobilities were measured using 3.5 eV photon energies as obtained for a tripled Nd:YAG laser with 5 ns pulse width. TOF signals were recorded using a liquid crystal cell with 10 μm spacing between the electrodes. Bottom and top electrodes consisted of tin-doped indium oxide, covered with a thin, rubbed polyimide orientation layer. Rubbing direction of the bottom and top contact were parallel. The cells were filled in an inert atmosphere utilizing the capillary force acting on the liquid-crystalline material in its nematic phase. Temperature-dependent current transients

(10) O'Neill, M.; Kelly, S. M. *Adv. Mater.* **2003**, *15*, 1135.
(11) Adam, D.; Schuhmacher, P.; Simmerer, J.; Haussling, L.; Siemensmeyer, K.; Etzbach, K. H.; Ringsdorf, H.; Haarer, D. *Nature* **1994**, *371*, 141.
(12) Funahashi, M.; Hanna, J. *Appl. Phys. Lett.* **2000**, *76*, 2574.
(13) Sirringhaus, H.; Wilson, R. J.; Friend, R. H.; Inbasekaran, M.; Wu, W.; Woo, E. P.; Grell, M.; Bradley, D. D. C. *Appl. Phys. Lett.* **2000**, *77*, 406.
(14) Yasuda, T.; Fujita, K.; Tsutsui, T.; Geng, Y.; Culligan, S. W.; Chen, S. H. *Chem. Mater.* **2005**, *17*, 264.
(15) Amundson, K. R.; Katz, H. E.; Lovinger, A. J. *Thin Solid Films* **2003**, *426*, 140.
(16) Zhang, H.; Shiino, S.; Shishido, A.; Kanazawa, A.; Tsutsumi, O.; Shiono, T.; Ikeda, T. *Adv. Mater.* **2000**, *12*, 1336.

Table 1. Phase Behavior of **6a**−**c** and Their Mixtures (K: crystalline, Sm: smectic, N: nematic, I: isotropic)

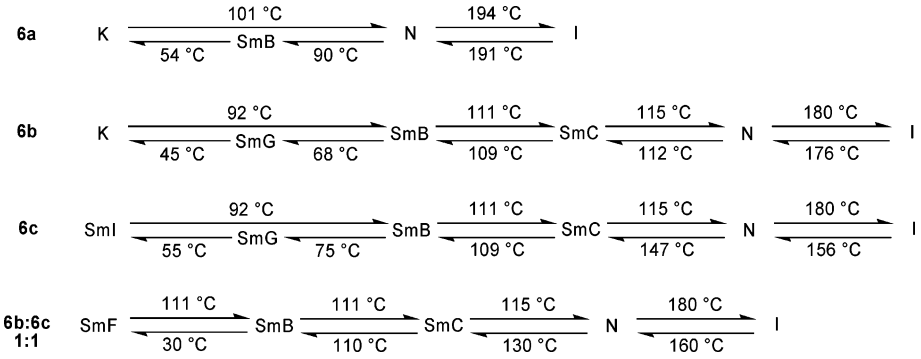

were measured by first heating the cells to the isotropic phase followed by slow (<10 deg/min) cooling to the temperature of interest. Processing and electrical characterization of the semiconductors was performed in ambient conditions. Bottom-gate transistors were prepared by spin-coating a 2 wt % solution of the semiconductor in toluene at a speed of 2000 rpm for 30 s on OFET test substrates. Heavily doped silicon was used as the gate electrode, with a hexamethyldisilazane (HMDS)-treated 200 nm thick layer of thermally oxidized SiO_2 as the gate insulating layer. Gold was thermally evaporated and patterned to form interdigitated source and drain contacts. Monodomain top-gate transistors were fabricated on ion-free glass substrates. Before the deposition of the semiconductor, an alignment layer was applied according to the following scheme:

(1) 1 mL of PI (AL 1051 from JSR, Japan) was dissolved in 3 mL of γ-butyrolacton,

(2) the substrate was fully covered with the PI-solution and spin-coated for 20 s at 3000 rpm.

(3) the PI was cured on a hot plate at 90°C for 1 h and then at 180 °C for 3 h.

(4) the layer was manually rubbed on a velvet cloth.

Source and drain electrodes were lithographically defined after the evaporation of a gold layer. The rubbed PI was then used as an alignment layer for the mesogen materials. A mesogen film was first applied by spin-coating and subsequently treated thermally. The optimized process for the monodomain formation of **6b** was the following:

(1) 10 mg of the semiconductor were dissolved in 1 mL toluene.

(2) the substrate with the rubbed polyimide was fully covered with the freshly prepared semiconductor solution.

(3) a thin film was obtained by spin-coating for 25 s at 1200 rpm.

(4) the substrate was placed into a hot stage that was continuously purged with dry nitrogen.

(5) the substrate was heated to 145 °C and then cooled to 30 °C at a rate of 5 °C/min.

After thermal treatment, an insulating layer of a fluorinated polymer (Teflon AF1600, DuPont) was spin-coated from FC75 (Acros), and the gold top-gate electrode was evaporated through a shadow mask. Single transistors were characterized at 40 °C in darkness, both in ambient atmosphere and in a vacuum using a HP4156B semiconductor parameter analyzer. Mobility statistics were obtained in ambient atmosphere and darkness.

General Procedure 5,5″-Bis(5-alkyl-2-thienylethynyl)-2,2′:5′,2″-terthiophenes, 6. To a mixture of 2-alkyl-5-trimethylsilylethynyl thiophene (19 mmol) in dry THF (50 mL) was added under N_2 TBAF on silica (21.6 g, 24 mmol). After 5 min the mixture was filtered over Celite and concentrated in vacuo. This material was immediately used in the next step.

To a degassed solution of dibromoterthiophene (3.05 g, 7.5 mmol) and 2-alkyl-5-ethynyl thiophene **5** (19 mmol) in diisopropylamine (60 mL) and THF (15 mL) was added $Pd(PPh_3)_4$ (260 mg, 0.22 mmol). The mixture was again degassed and heated for 15 min at 40 °C. Subsequently, CuI (100 mg, 0.52 mmol) was added, and the mixture was heated at reflux for 18 h. The solution was allowed to cool to room temperature, CH_2Cl_2 (100 mL) was added, and the precipitate was filtered off over Celite. The filtrate was concentrated in vacuo, purified by column chromatography on silica using hexane−CH_2Cl_2 followed by recrystallization from hexane.

5,5″-Bis(5-butyl-2-thienylethynyl)-2,2′:5′,2″-terthiophene, 6a. This product was prepared according to the general procedure and obtained as an orange-red powder (3.1 g, 72%). Thermal behavior: see Table 1. ^{1}H NMR ($CDCl_3$, δ): 0.89 (t, 6H, CH_3), 1.2−1.4 (m, 12H, $-CH_2-$), 1.67 (m, 4H, $-CH_2-$), 2.80 (t, 4H, ar·CH_2-), 6.68 (d, 2H, ar·H), 7.04−7.16 (m, 8H, ar·H). ^{13}C NMR ($CDCl_3$, δ): 14.00, 22.23, 30.00, 33.69, 85.42, 88.30, 119.88, 122.14, 123.63, 124.31, 124.83, 132.34, 132.66, 136.02, 138.27, 149.08. Anal. Calcd for $C_{28}H_{28}S_5$: C, 67.09; H, 4.93; S, 27.98. Found: C, 67.13; H, 4.98; S, 27.89.

5,5″-Bis(5-hexyl-2-thienylethynyl)-2,2′:5′,2″-terthiophene 6b. This product was prepared according to the general procedure and obtained as orange fluffy crystals (3.8 g, 80%). Thermal behavior: see Table 1. ^{1}H NMR ($CDCl_3$, δ): 0.89 (t, 6H, CH_3), 1.3−1.5 (m, 4H, $-CH_2-CH_3$), 1.66 (m, 4H, $-CH_2-$), 2.81 (t, 4H, ar·CH_2-), 6.68 (d, 2H, ar·H), 7.05−7.16 (m, 8H, ar·H). ^{13}C NMR ($CDCl_3$, δ): 14.05, 22.54, 28.69, 30.22, 31.47, 31.51, 85.40, 88.27, 119.87, 122.14, 123.61, 124.33, 124.83, 132.34, 132.68, 136.01, 138.29, 149.07. Anal. Calcd for $C_{44}H_{52}S_5$: C, 68.74; H, 5.77; S, 25.49. Found: C, 68.67; H, 5.72; S, 25.61.

5,5″-Bis(5-decyl-2-thienylethynyl)-2,2′:5′,2″-terthiophene 6c. This product was prepared according to the general procedure and obtained as a red-orange solid (4.3 g, 77%). Thermal behavior: see Table 1. ^{1}H NMR ($CDCl_3$, δ): 0.88 (t, 6H, CH_3), 1.1−1.4 (m, 28H, $-CH_2-$), 1.67 (m, 4H, $-CH_2-$), 2.79 (t, 4H, ar·CH_2-), 6.69 (d, 2H, ar·H), 7.04−7.16 (m, 8H, ar·H). ^{13}C NMR ($CDCl_3$, δ): 14.10, 22.67, 29.03, 29.31 (2 C-atoms), 29.53, 29.57, 30.23, 31.52, 31.88, 85.39, 88.28, 119.88, 122.18, 123.63, 124.34, 124.85, 132.35, 132.68, 136.04, 138.29, 149.11. Anal. Calcd for $C_{44}H_{52}S_5$: C, 71.30; H, 7.07; S, 21.63. Found: C, 71.21; H, 6.97; S, 21.82.

3. Results and Discussion

Synthesis. The new liquid-crystalline semiconductors **6b** and **6c** were targeted to study in detail the phase behavior, monodomain formation, and electrical transport. These materials can be conveniently synthesized according to the procedure outlined in Scheme 1. Thus, alkylation of thiophene by means of lithiation and quenching with an alkylbromide gave the monoalkylthiophenes **2** in 75% yield. These were subsequently brominated with *N*-bromosuccinimide to afford intermediates **3** in 90% yield, which were converted to **4** using trimethylsilylacetylene in a Sonogashira[17] coupling in 80% yield. Deprotection with tetrabutylammoniumfluoride on silica afforded the

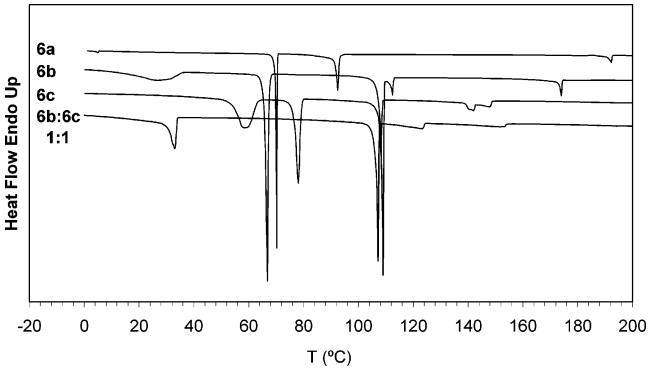

Figure 1. DSC traces (cooling run) of mesogens **6a**−**c** and 1:1 mixture of **6b** and **6c**.

acetylenes **5** in nearly quantitative yield, which were directly coupled with dibromoterthiophene, yielding the bis(5-alkyl-2-thienylethynyl)-2,2′:5′,2″-terthiophenes **6** in 80% yield. The overall yield of this synthesis route was typically 40−45%.

Phase Behavior and Identification. The DSC traces and phase transition temperatures of the calamitic compounds **6a**−**c** and the 1:1 mixture of **6b** and **6c** are collected in Figure 1 and Table 1, respectively.

The determination and assignment of the mesophases were carried out using differential scanning calorimetry (DSC) and optical microscopy. All the compounds exhibit a nematic liquid-crystalline phase at an elevated temperature. The clearing temperature, the transition from the nematic to the isotropic phase, decreases with increasing length of the alkyl side chain of the compounds. Only the compounds with the longest alkyl chains, hexyl derivative **6b** and decyl derivative **6c**, give rise to a smectic C phase. The transition of the nematic to SmC phase shows the typical bars under polarizing optical microscopy.[18] As for the butyl-substituted derivative, **6a**, the SmB phase of **6b**, **6c**, and their 1:1 mixture display a mosaic texture. Upon further cooling, molecules **6b** and **6c** show a highly ordered SmG phase, which is missing for **6a** and for the 1:1 mixture of **6b** and **6c**. Only the compounds **6a** and **6b** exhibit a crystalline phase.

Monodomain Formation. To study the ability of monodomain formation, thin films of the compounds were made by spin-coating a toluene solution on rubbed polyimide. Annealing the substrate to the nematic phase of the compound (145 °C) and gradual cooling (5 °C/min) to 30 °C, resulted in the formation of a monodomain in the size of the substrate. Using this process we were able to produce monodomains of up to 150 mm in diameter (see Figure 2).

Figure 3 presents the result of polarized light microscopy on an as-spun and an annealed film of **6b**. During spin-coating on rubbed polimide, the mesogen crystallized in the form of needles, which can be observed in Figure 3a. Upon heating to the nematic phase, the mesogen self-organizes into a monodomain. This monodomain is maintained upon cooling and passing through the SmC-, SmB-, and SmG phases. At about 45 °C, crystallization starts at one side of the substrate. There appears to be a cooperative effect, as the solid monodomain grows from one side of the substrate to the other side. Under crossed polarizers, this process can be observed as a gradual

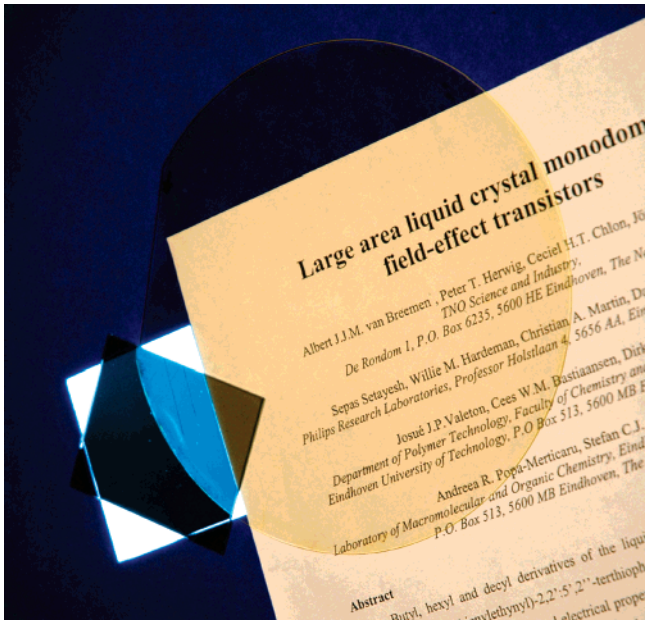

Figure 2. Photograph of a 150-mm monodomain of **6b** illuminated from the back. The lower left of the wafer is placed between two crossed linear polarizers. The enhanced transmission through the monodomain illustrates the dichroism and uniformity of the ordered film.

darkening of the film. During this crystal growth, no grain boundaries are formed, and hence the monodomain is maintained. Figure 3b−d depicts such a monodomain for different rotation angles versus the polarization plane of the illumination. While the uniform brightness indicates the absence of domain boundaries in the films, the optical anisotropy gives an indication of the order and the molecular alignment, which will be discussed in more detail in the next section.

Although all compounds studied here display, upon cooling from the isotropic phase, a sequence of phases with increasing order, only defect-free monodomains at room temperature could be made from **6b**, **6c**, and the 1:1 mixture of **6b** and **6c**. These (mixtures of) compounds all show a slow transition to either the crystalline phase (**6b**), the SmI phase (**6c**), or the SmF phase (1:1 mixture of **6b** and **6c**). This is in contrast to the sharp peak observed in DSC for the crystallization of **6a** at about 50 °C (see Figure 1). During this transition a lot of defects are introduced in the monodomain. Apparently, the slow transition found in **6b**, **6c**, and the 1:1 mixture of **6b** and **6c** is essential for the preservation of defect-free monodomains when cooling to room temperature. Furthermore, the layer thickness was, in general, found to be essential for monodomain formation, a fact which must be attributed to the anchoring strength of the rubbed PI. Its influence on the long-range order of the mesogen is only maintained for the critical thickness,[19] beyond which the monodomain order is lost and the material self-organizes in multiple domains. In practice this means that for layer thicknesses below 150 nm, monodomains can be formed in a reproducible way.

Polarized UV Absorption. The UV/vis absorption spectrum of **6b** in toluene is presented as an inset in Figure 4. It shows two distinct absorption bands, one at a wavelength of 424 nm (2.93 eV) and another at 311 nm (3.99 eV). The long wavelength

(17) Sonogashira, K.; Tohda, Y.; Hagihara, N. *Tetrahedron Lett.* **1975**, *16*, 4467.
(18) Demus, D.; Richter, L. *Textures of Liquid Crystals*; Verlag Chemie: Weinheim, 1978.
(19) Collings, P. J.; Patel, J. S. *Handbook of Liquid Crystal Research*; Oxford University Press: New York, 1997.

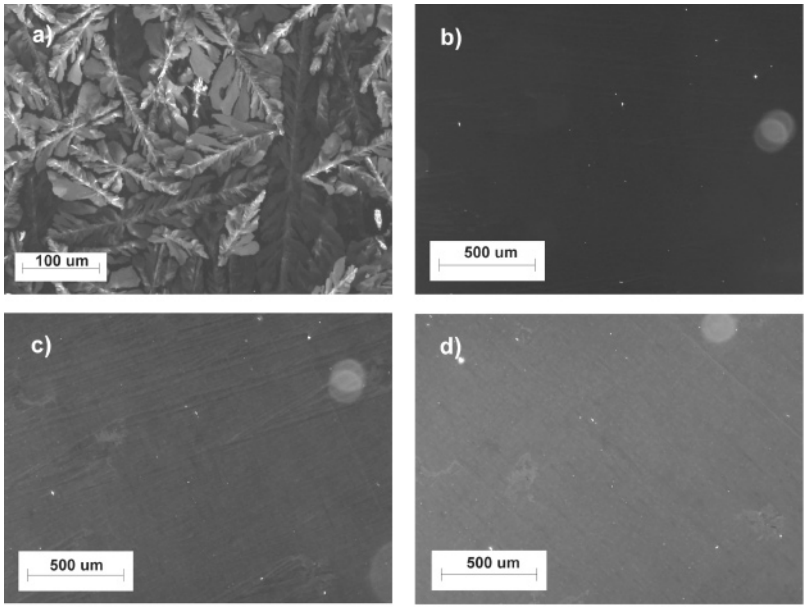

Figure 3. Light transmission micrographs of two films of compound **6b** (polarizer in the horizontal, analyzer in the vertical direction): (a) untreated, as-spun film; (b) monodomain with the rubbing direction of the PI layer parallel to the analyzer; (c) rubbing direction at 22.5° with respect to the analyzer; (d) rubbing direction at an angle of 45° with respect to the analyzer.

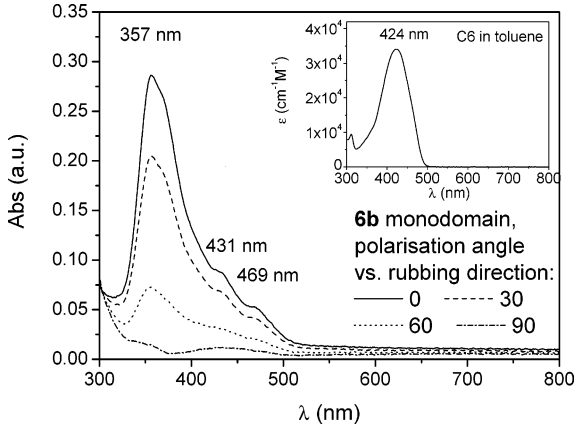

Figure 4. Absorbance of a monodomain of **6b** on a glass/rubbed PI substrate as a function of probe beam polarization. Film thickness: 50 nm. (Inset) Molar absorption coefficient in toluene as a function of wavelength.

band is a dipole-allowed, $\pi-\pi^*$ absorption band of the conjugated π-electron system of the core of the mesogens. This band corresponds to the transition from the ground state to the lowest excited singlet state of the molecule. The position of this band matches sufficiently well with the long wavelength absorption band of alkyl-substituted quinquethiophene in chloroform, which has been reported at 420 nm.[20] The second absorption band at 311 nm corresponds to a transition to a higher-lying singlet state.

The absorption spectra of monodomain thin films of **6b** differ significantly from those of the isolated molecules in solution. A plot of the monodomain absorbance at different polarization angles with respect to the PI rubbing direction is presented in Figure 4. For an angle of 0°, the overall film absorbance is at a maximum. Here, the spectrum displays a single peak at 357 nm and two shoulders at 431 and 469 nm. Comparison with the absorption in solution reveals both a blue-shift of the maximum and a simultaneous red-shift of the onset. These changes are often observed for oligothiophenes upon the formation of aggregates[21] or microcrystals, and these features have also been observed in crystalline quinquethiophene films.[22] The changes in the spectra can be rationalized in terms of formation of H-aggregates. Here the close proximity and side-to-side arrangement of the oligothiophene chromophores gives rise to relatively strong interactions between the transition dipole moments of the chromophoric units. This results in excited states which are delocalized over a significant number of molecules with the transition from the ground state and the lowest-energy delocalized states being dipole-forbidden in nature.

For polarization angles >0° the overall absorbance of the monodomain is reduced and reaches a minimum at an angle of 90°. At 357 nm, the dichroic ratio, i.e. the ratio of maximum to minimum absorption, is as large as 19. Since the maximum transition dipole moment in oligothiophenes can be expected to be aligned along their backbone,[22] this result suggests that the **6b** molecules are aligned or tilted in the direction of the rubbing. By rocking the sample around an axis perpendicular to the rubbing, a further increase in absorption was observed for 0° degrees polarization angle. This indicates that the molecules are not oriented perfectly perpendicular to the substrate but that all molecules in the film are tilted in the direction of the rubbing.

It is well-known that, in first approximation, the dipole strength of an absorption band is conserved when comparing isolated and interacting molecules.[23] This allows us to obtain an estimate of the tilt angle of molecules by evaluating the area under the absorption curve of the monodomain and comparing

(20) Barbarella, G.; Favaretto, L.; Zambianchi, M.; Pudova, O.; Arbizzani, C.; Bongini, A.; Mastragostino, M. *Adv. Mater.* **1998**, *10*, 551.

(21) Schenning, A. P. H. J.; Kilbinger, A. F. M.; Biscarini, F.; Cavallini, M.; Cooper, H. J.; Derrick, P. J.; Feast, W. J.; Lazzaroni, R.; Leclere, Ph.; McDonell, L. A.; Meijer, E. W.; Meskers, S. C. J. *J. Am. Chem. Soc.* **2002**, *124*, 1269.

(22) Kanemitsu, Y.; Shimizu, N.; Suzuki, K.; Shiraishi, Y.; Kuroda, M. *Phys. Rev. B* **1996**, *54*, 2198.

(23) See, e.g.: Harada, N.; Nakanishi, K. *Circular Dichroic Spectroscopy: Exciton Coupling in Organic Stereochemistry*; University Science Books: Mill Valley, CA; Oxford University Press: Oxford, UK, 1983.

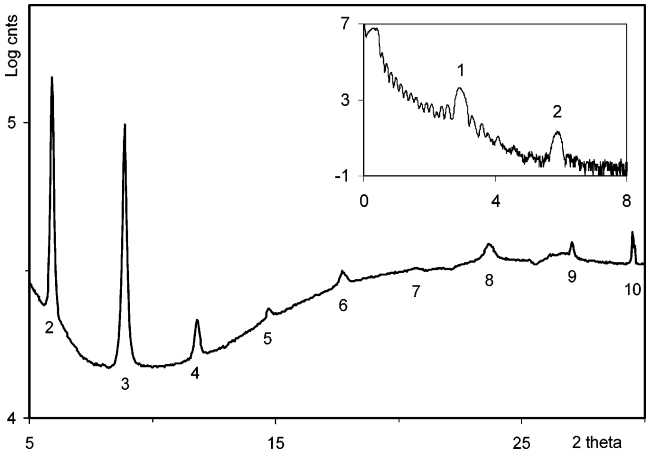

Figure 5. Wide angle (WAXS) specular Θ/2Θ scan of a monodomain of **6b**. (Inset) Typical X-ray reflection scan.

this with isotropically averaged dipole strength of the isolated molecules as observed in toluene solution. For compound **6b** in toluene we obtain a dipole strength of 48 D^2 and hence a transition dipole moment of 7 D when including a correction for the Lorentz local field in the solvent ($n = 1.5$) cage around the molecule.[24] For the thin monodomain film we find that the projection of the transition dipole moment in the plain of the film along the rubbing direction amounts to 4.6 D. This implies an angle between the transition dipole moment of the molecule and the in-plane rubbing direction of approximately 50°.

Microstructure of Monodomains. The microscopic order in the monodomains was investigated with X-ray diffraction. A wide angle (WAXS) specular Θ/2Θ scan is presented in Figure 5. The diffraction peak at 5.93° can be assigned to the 200 reflection. Peaks at larger angles are due to higher-order reflections, up to the 10th order. The observed order in one dimension of this highly layered structure corresponds to at least a liquid-crystalline phase, but possibly a crystalline phase. There are no other lattice planes parallel to the substrate. The interplanar spacing amounts to 30.1 Å. The length of the molecule as calculated with ChemDraw3D is 37 Å. When we assume that the packing of the molecules (or mesogens) is comparable to that of compound **6a**,[25] we can estimate that the molecules are tilted with respect to the polyimide alignment layer under an angle of about 54°, a value that is supported by the tilt calculated from the absorption measurements. A detailed analysis of the in-plane order using pole figure measurements will be published elsewhere. The small-angle reflections are shown in the insert in Figure 5. The insert shows the 100, 200, and 300 diffraction peaks and the total internal reflection and a number of interference, or Kiessig,[26] fringes. Interpretation of the fringes, i.e. determination of polyimide- and mesogen **6b** layer thickness and roughness, was not attempted.

Topography of Monodomains. The surface roughness of the monodomains was analyzed with atomic force microscopy (AFM) in noncontact tapping mode using scan lengths, L, from 80 to 2 μm. A micrograph of 20 μm scan length is presented in Figure 6. The rubbing direction of the polyimide corresponds with the horizontal direction. The micrographs show elevated

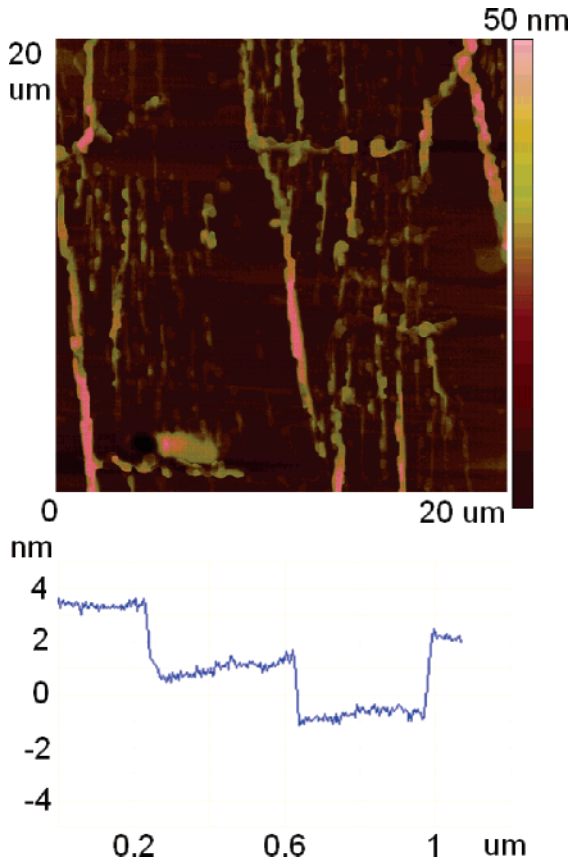

Figure 6. (Upper image) Atomic force micrograph of a monodomain of **6b**. The polyimide rubbing direction is parallel to the horizontal axis. The topography shows elongated fibrils perpendicular to the rubbing direction and lamellae parallel to the rubbing direction. (Lower figure) Typical height profile observed at small scan lengths. The profile shows discrete steps whose height corresponds to the interplanar spacing of 30 Å.

fibrils perpendicular to the rubbing direction, and an underlying structure of lamellae parallel to the rubbing direction. Height profiles measured at small scan lengths show discrete steps. A typical example is given in the lower part of Figure 6. The height of the steps corresponds to the interplanar spacing of 30 Å as obtained from WAXS measurements. Hence, the monodomain grows as a stack of discrete monolayers. The origin of the fibrils is not yet known; they might be due to changes in the orientation during crystal growth.

The height profiles were analyzed from the power spectral density (PSD) as a function of the spatial frequency, f.[27] The PSD is calculated by using eq 1, taking scan lengths, L, from 80 to 2 μm both parallel and perpendicular to the polyimide rubbing direction. The calculated PSD is presented in Figure 7.

$$\mathrm{PSD}(f) = \frac{1}{L}\left[\int_0^L h(x)\exp(i2\pi f x)\,dx\right]^2$$

with

$$\alpha = \frac{(\gamma - d)}{2} \qquad (1)$$

Both horizontal and vertical PSD scans show that for each scan length the height fluctuations are spatially correlated. The top graph shows uncorrelated behavior or a white spectrum at low

(24) Michl, J.; Thulstrup, E. W. *Spectroscopy with Polarized Light*; VCH: New York, 1986.
(25) Zhang, H.; Shiino, S.; Kanazawa, A.; Tsutsumi, O.; Shiono, T.; Ikeda, T.; Nagase, Y. *Synth. Met.* **2002**, *126*, 11.
(26) Kiessig, H. *Ann. Phys.* **1931**, *10*, 769.
(27) Biscarini, F.; Samori, P.; Greco, O.; Zamboni, R.; *Phys. Rev. Lett.* **2002**, *78*, 2389.

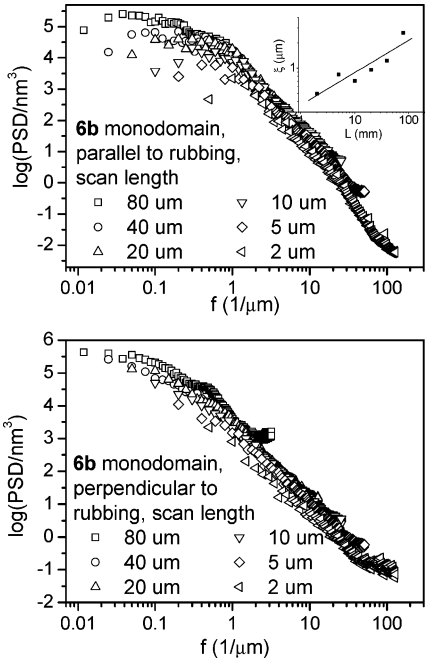

Figure 7. Power spectral density (PSD) of the monodomain topography from AFM images of different scan lengths, L, from 80 μm through 2 μm. Top and bottom figures correspond respectively to the scan direction parallel and perpendicular to the rubbing direction. (Inset in top figure) Estimated correlation length ξ versus the scan length L. The solid line is a power law fit.

frequencies. However, this plateau spans only a few points, suggesting that the apparent breakdown of correlations is partly due to the finite AFM image size.[28] This interpretation is supported by the inset showing an increase of the estimated correlation length (viz. the inverse of the breakdown frequency separating the power law decay from the apparent plateau) with the scan length L. A power law fit yielded $\xi \approx L^{0.38}$, while a linear dependence would be expected for the ideal case. We note that the scans perpendicular to the rubbing direction do not show a plateau related to the image size. Hence, the origin of the loss of correlation at low spatial frequencies for the parallel scan direction remains unclear. It might also be due to the fibrils (see Figure 6). These protrusions run perpendicular to the rubbing direction and, therefore, the height profiles on both sides are not correlated. This is supported by the values obtained for the coherence length.[27] The coherence length in the rubbing direction is about 2−5 μm, comparable to the distance between the fibrils. The coherence length perpendicular to the rubbing direction is estimated to be larger by an order of magnitude.

Figure 7 shows that the PSD scales over more than 5 decades with spatial frequency. This indicates that height fluctuations are spatially correlated. The topography of the monodomains shows anisotropic or self-affine scaling.[27] Similar scaling behavior has been observed for, e.g. plasma-deposited polymer films[29] and thin films of oligothiophenes.[27,28,30] The power law exponent is related to the static scaling parameter α via eq 1, where the scan dimension d is equal to unity. For both scanning directions a value for α of about 0.6−0.7 is obtained. This might indicate that the growth mechanism of the monodomains is dominated by adsorption of molecules on kink sites similar to those observed for MBE-grown films.[27,31]

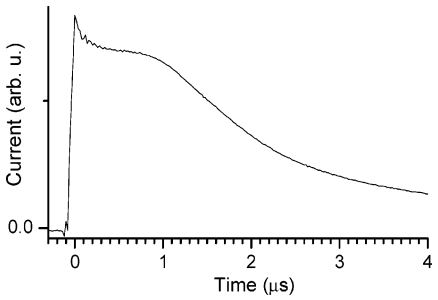

Figure 8. Time-of-flight photocurrent transients for **6b** with 10 μm electrode spacing, 3.5 eV photon energy, and $T = 100$ °C, transport due to holes. Electric field strength 4×10^4 V/cm.

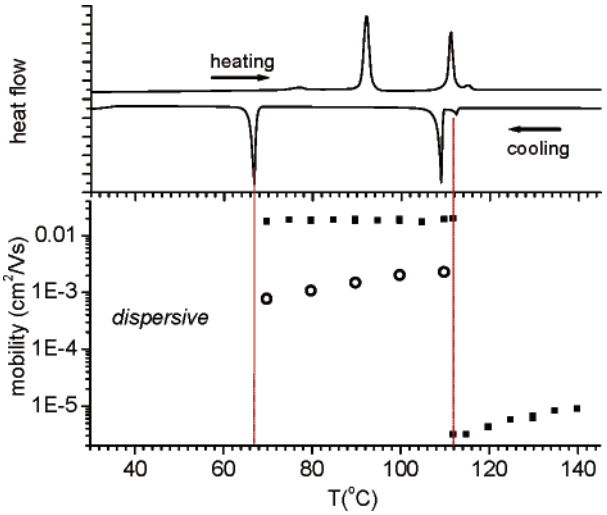

Figure 9. (Lower part) Time-of-flight mobility for **6b** as a function of temperature. (■) Holes. (○) Electrons. Electric field 4×10^4 V/cm, path length: 10 μm. (Upper part) DSC trace for **6b** indicating the various phase transitions.

Electrical Transport Measurements. To evaluate the mobility of charge carriers in the bulk of the mesogenic material we have used conventional time-of-flight (TOF) mobility measurements. Figure 8 shows the TOF photocurrent transients for **6b** for positive charge carriers in the SmB phase. After excitation at $t = 0$, the arrival time of the holes at the electrode opposite to the side of illumination is clearly marked by a kink in the photocurrent at $t = 1.1$ μs.

For compound **6b**, slow charge carrier transport ($\mu = 10^{-5}$ cm^2/Vs) is observed in the nematic phase of the material (Figure 9). Such low mobilities at high temperatures agree with the behavior of other mesogens and may be interpreted in terms of transport of ionized impurities in the low-viscosity phases.[32] Upon lowering the temperature for **6b**, almost nondispersive transport and high carrier mobilities are observed in the SmB phase. Here, the hole mobility amounts to 2×10^{-2} cm^2/Vs and is almost independent of the applied field and temperature and shows a negligible variation with the intensity of the light pulse. The hole mobility found is slightly higher than that reported for alkyl-functionalized terthiophenes.[12] Mobilities for electrons (1.2×10^{-3} cm^2/Vs, $T = 80$°C, electric field strength

(28) Melucci, M.; Gazzano, M.; Barbarella, G.; Cavallini, M.; Biscarini, F.; Maccagnani, P.; Ostoja, P. *J. Am. Chem. Soc.* **2003**, *125*, 10266.
(29) Collins, G. W.; Letts, S. A.; Fearon, E. M.; McEachern, R. L.; Bernat, T. P. *Phys. Rev. Lett.* **1994**, *73*, 708.
(30) Biscarini, F.; Zamboni, R.; Samorí, P.; Ostoja, P.; Taliani, C. *Phys. Rev. B* **1995**, *52*, 14868.
(31) Lai, Z.-W.; Das Sarma, S. *Phys. Rev. Lett.* **1991**, *66*, 2348.

$E = 3 \times 10^4$ V/cm) are almost 1 order of magnitude lower than those for holes (1.7×10^{-2} cm^2/Vs, $T = 80$°C, $E = 3 \times 10^4$ V/cm) and increase with temperature (see Figure 9). Similar differences between electron and hole transport have been observed in other smectic organic semiconductors, where the differences were attributed to different transport mechanisms.[33] In the latter case, electron transport was found to be limited by shallow trap levels. Upon further lowering the temperature below the phase transition between the SmB and SmG phase, the current transient becomes strongly dispersive, which we attribute to the scattering effects of grain boundaries. Optical microscopy showed that for these thick films (10 μm) domains of limited spatial extent are formed, in contrast to thin films which can form large monodomains.

Mobilities for compound **6c** are almost the same as for **6b** ($\mu_{hole} = 1.9 \times 10^{-2}$ cm^2/Vs, $\mu_{electron} = 2.4 \times 10^{-3}$ cm^2/Vs, $T = 100$° C, $E = 3 \times 10^4$ V/cm). Interestingly, for a mixture of **6b** and **6c** (1:1 by weight), mobilities are comparable to those of the pure compounds ($\mu_{hole} = 1.1 \times 10^{-2}$ cm^2/Vs, $\mu_{electron} = 1.4 \times 10^{-3}$ cm^2/Vs, $T = 80$°C, $E = 3 \times 10^4$ V/cm) Apparently, the disorder introduced by mixing the two different mesogens does not affect the charge carrier transport. This may be related to the fact that the difference in chemical structure between the two mesogens is located in the side chains far away from the central π-conjugated moiety.

To investigate the electrical performance of thin films from the LC semiconductor **6b** and to compare it to previous results on mesogen devices, thin-film transistors in the bottom- and top-gate architecture were prepared. Spin-coating of **6b** on bottom-gate substrates led to the formation of multiple domains with sizes on the order of several micrometers. Similar results have been reported for other mesogens deposited without alignment layers. Arrangement of mesogens in such multidomains usually prevents full exploitation of their semiconducting properties in thin-film transistors.[34]

A detrimental influence of the domain boundaries could also be observed in our samples. The transfer characteristics of a representative bottom-gate transistor from **6b** in a vacuum are given in Figure 10. Above a gate bias of approximately 0 V, the depletion of the semiconductor layer leads to a drain current on the order of 100 pA. The remaining current can be attributed to parasitic conduction from the gate probe, which, in this setup, cannot be shielded from the semiconductor film. For a gate bias below 0 V, the drain current increases rapidly. Microscopically, this effect corresponds to the build-up of an accumulation channel at the interface to the insulator. As V_g is decreased further, the current increases to reach a maximum value of 3 μA in the saturated regime, leading to an on/off ratio of more than 10^4. However, the counterclockwise hysteresis in the transfer characteristics is rather large and might be attributed to the presence of trapping sites at domain boundaries or to states at the semiconductor−dielectric interface.[35]

Figure 10 also displays the hole mobilities of the transistor. The mobility for a drain bias of $V_d = -5$ V, i.e., in the linear regime, was calculated according to

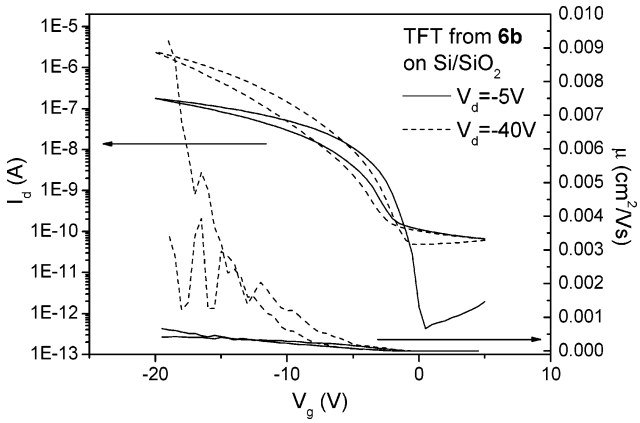

Figure 10. Transfer characteristics of a transistor with interdigitated electrodes, prepared from **6b** in the bottom-gate architecture. The channel width was 10 mm, the length was 10 μm. The device was measured in a vacuum.

$$\mu_{lin} = \frac{L}{V_d W C_i'} \frac{\partial I_d}{\partial V_g} \tag{2}$$

For maximum hole accumulation at $V_g = -40$V it is around 5×10^{-4} cm^2/Vs. This value is much lower than the mobility in the saturated regime, which is given by

$$\mu_{sat} = \frac{L}{W C_i'} \frac{\partial^2 I_d}{\partial V_g^2} \tag{3}$$

and which amounts to approximately 0.004 cm^2/Vs. The difference can be attributed to an injection limitation in the device, which will be addressed later. In the following, the saturated mobility will be used for discussion. For the device presented in Figure 10 it is on the order of the values reported for other mesogen multidomain TFTs by McCulloch and coworkers,[34] but far from the mobility achieved in the TOF measurements. Hence, the device geometry was adapted to improve the order in the semiconductor films.

In the resulting top-gate architecture the Au source and drain contacts were located on top of a PI layer, rubbing of which enabled the alignment of the LC semiconductor. In these devices, spin-coating and annealing of a film of **6b** (see Experimental Section) was followed by spin-coating the gate dielectric and evaporation of the gate electrode. Control samples in which the PI was not rubbed exhibited a performance similar to the bottom-gate devices presented earlier, with saturated mobilities reaching 0.004 cm^2/Vs and trapping-dominated hysteresis. Full exploitation of the electrical properties of **6b** was only possible in top-gate devices with a rubbed PI layer. Here, the alignment of the LC semiconductor led to monodomain TFTs with a significant improvement in mobility and a decrease in hysteresis.

Figure 11 presents the transfer characteristics of a typical monodomain top-gate transistor with interdigitated electrodes. The device exhibits a large on/off ratio of approximately 10^6 in the saturated regime. To a large extent, this high performance is due to the significantly small off current of 10 pA. A further benefit of the top-gate architecture is illustrated by the extremely small hysteresis in the displayed transfer characteristics. The

(32) Funahashi, M.; Hanna, J. *Chem. Phys. Lett.* **2004**, *397*, 319.
(33) Shiyanovskaya, I.; Singer, K. D.; Twieg, R. J.; Sukhomlinova, L.; Gettwert, V. *Phys. Rev. E* **2002**, *65*, 041715.
(34) McCulloch, I.; Zhang, W.; Heeney, M.; Bailey, C.; Giles, M.; Graham, D.; Shkunov, M.; Sparrowe, D.; Tierney, S. *J. Mater. Chem.* **2003**, *13*, 2436.
(35) Zilker, S. J.; Detcheverry, C.; Cantatore, E.; de Leeuw, D. M. *Appl. Phys. Lett.* **2001**, *79*, 1124.

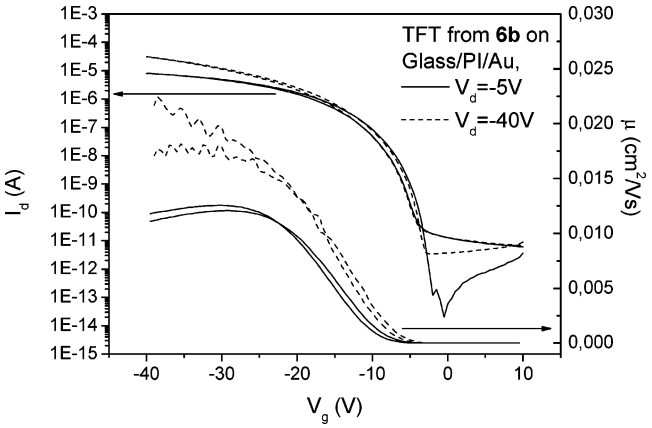

Figure 11. Transfer characteristics of a monodomain top-gate TFT with its channel perpendicular to the rubbing direction of the alignment layer. The channel width was 20 mm, the length was 20 μm. The device was measured in a vacuum.

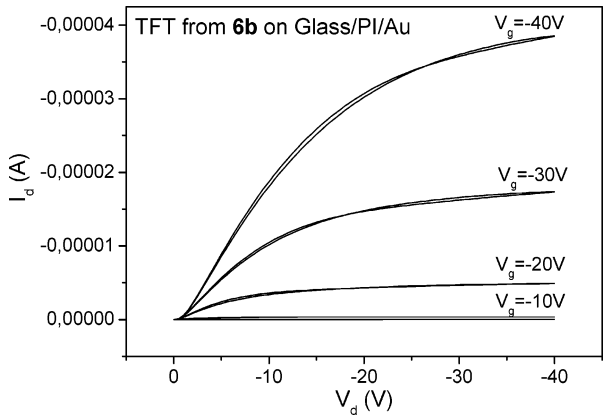

Figure 12. Output characteristics of the same monodomain top-gate TFT as displayed in Figure 11. The device was measured in a vacuum.

absence of domain boundaries reduced the number of trapping sites in the device significantly.

This also led to an increase in mobilities compared to the bottom-gate TFTs. In the linear regime the top-gate device displayed in Figure 11 exhibits a mobility around 0.01 cm^2/Vs, which is slightly smaller than the value in saturation. As discussed earlier, this difference can be attributed to an injection limitation in the device, which might be due to a mismatch of the HOMO level of **6b** and the work function of the source and drain electrodes. It is further illustrated by the output characteristics of the device (see Figure 12), which display a superlinear current onset.

The saturated mobility in the monodomain TFT is as large as 0.02 cm^2/Vs and hence by almost an order of magnitude larger than that in multidomain devices. This also led to an increase in the saturated mobility compared to that of the bottom-gate TFT, which is as large as 0.02 cm^2/Vs in the monodomain devices. It is in good agreement with the hole mobility obtained from the TOF experiments, which often represents an upper limit to the transport properties in FETs.[36] The result exceeds the values reported for other reactive and nonreactive mesogens by far[34] and is on the order of the highest value reported for LC TFTs.[13,14] Furthermore, it is close to that of evaporated alkyl-substituted oligothiophenes. For bottom-gate transistors from α,α'-bisdecyl-sexithiophene, hole mobilities on the order of 0.1 cm^2/Vs and on/off ratios of 10^5 have been reported.[37] Evaporation of α,α'-bishexyl-sexithiophene, in contrast, has led to comparable mobilities, but much lower on/off ratios.[38]

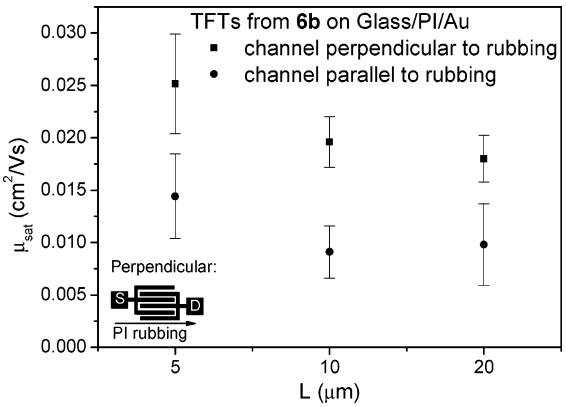

Figure 13. Statistical results of the saturated mobilities of devices of **6b**. The squares give the resulting mean mobility as a function of channel length, and the bars mark the standard deviation.

Within the experimental error, the mobility in monodomain transistors was found to be independent of channel width and considerably consistent throughout the sample. Figure 13 displays the saturated mobility in TFTs as a function of channel length. In the devices based on **6b** the saturated mobility in channels perpendicular to the rubbing direction of the polyimide is by a factor of 1.2−3.3 larger than that parallel to the rubbing.

Electrical anisotropy has also been reported in the LC copolymer transistors fabricated by Sirringhaus and co-workers.[13] There, the mobility values in the direction of the conjugated backbone were by a factor of 10 larger than those in the direction perpendicular to the molecule chains. However, faster intramolecular charge transport processes cannot account for the results in the case of **6b**. Both parallel and perpendicular to the rubbing direction, hole transport in the **6b** monodomain is mainly governed by intermolecular charge transfer. Possible differences in the electrical properties of the bulk can merely be induced by differing π-orbital overlaps. These could either be due to the tilt of the molecules revealed by optical analyses, or due the rotational asymmetry of the backbone of **6b**. Another origin of the mobility anisotropy in the field-effect transistors might be found in the increased surface roughness of the **6b** monodomain in the direction of the rubbing. The extent of the individual contributions of surface and bulk properties is not accessible without further information about the microstructure of the material.

Overall, the saturated mobility displayed in Figure 13 seems to be largest for the smallest channel length. The output characteristics of devices with several channel lengths revealed short-channel effects, a phenomenon which has already been observed in other organic TFTs.[39] As a consequence of the large longitudinal electric field in the channel, the ideal equation employed for the mobility analysis does not hold, and the saturated mobility might be overestimated.

(36) Dimitrakopoulos, C. D.; Malenfant, P. R. L. *Adv. Mater.* **2002**, *14*, 99.
(37) Halik, M.; Klauk, H.; Zschieschang, U.; Schmid, G.; Radlik, W.; Ponomarenko, S.; Kirchmeyer, S.; Weber, W. *J. Appl. Phys.* **2003**, *93*, 2977.
(38) Deman, A.-L.; Tardya, J.; Nicolas, Y.; Blanchard, P.; Roncali, J. *Synth. Met.* **2004**, *146*, 365.
(39) Chabinyc, M. L.; Lu, J.-P.; Street, R. A.; Wu, Y.; Liu, P.; Ong, B. S. *J. Appl. Phys.* **2004**, *96*, 2063.

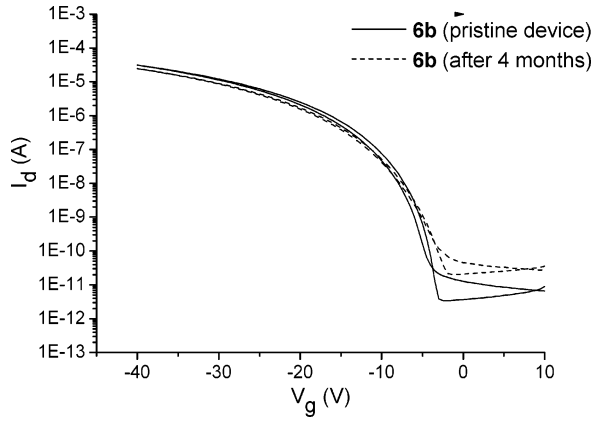

Figure 14. Transfer characteristics of **6b** as a function of time. Devices were stored at room temperature in ambient conditions.

To investigate the stability of the compound **6b**, some devices were again measured after prolonged storage in ambient conditions (see Figure 14). The devices were found to be stable, with mobility changes of less than 10% after three months in air and darkness. This good stability might be attributed to the absence of domain boundaries which, in the case of pentacene, have shown to be sensistive to degradation by water.[40] Furthermore, the position of the HOMO level is important for the stability of organic semiconductors against oxidative doping.[34] For **6b** a value of 5.7 eV vs vacuum was measured, which is apparently large enough to prevent degradation of the TFT characteristics on the time scale studied.

4. Conclusion

Butyl, hexyl, and decyl derivatives of the solution-processable compound 5,5″-bis(5-alkyl-2-thienylethynyl)-2,2′:5′,2″-terthiophene were synthesized to target self-organized semiconductor films for the application in large-area organic electronic devices. The phase behavior of the molecules with hexyl and decyl spacer groups was found to be ideal for the formation of highly ordered monodomains on an alignment layer of rubbed PI. Due to the slowly increasing order of their smectic mesophases and due to a stable crystalline phase at room temperature it was possible to process these compounds and their mixtures into monodomains of up to 150 mm in diameter. The order in these domains was confirmed by X-ray diffraction measurements, AFM studies and absorption spectroscopy, which suggest a side-to-side arrangement of the molecules in lamellae parallel to the substrate. Within these lamellae, the molecules are tilted in the rubbing direction of the underlying PI layer at an angle of roughly 40−50 degrees versus the plane normal.

The semiconducting properties of the compounds were studied by time-of-flight and transistor measurements. The hexyl compound showed the best bipolar transport properties, with maximum hole and electron TOF mobilities of 0.02 and 0.002 cm^2/Vs, respectively. This compound was further processed into top-gate monodomain field-effect transistors. Only this geometry allows the full exploitation of the self-organization of the liquid-crystalline semiconductor. Hole mobilities in this architecture reached up to 0.02 cm^2/Vs and were by 1 order of magnitude larger than those in multidomain bottom-gate devices. They were found to be stable for at least 3 months in ambient conditions. The mobility in monodomain transistors was anisotropic by a factor of about 2, with enhanced transport in the direction perpendicular to the rubbing of the PI alignment layer. A possible origin of this anisotropy can be found in both the bulk packing and in the surface properties of the monodomain, which showed the smoothest features in the direction perpendicular to the rubbing direction.

In terms of phase behavior, the studied 5,5″-bis(5-hexyl-2-thienylethynyl)-2,2′:5′,2″-terthiophene must be regarded as an ideal model compound for self-organizing liquid-crystalline organic semiconductors. On the other hand, the monodomain transistor mobility was similar to the transport data in TOF experiments and might therefore mark an intrinsic performance limit of this material. We anticipate, however, that this study paves the way for further improvement of the performance of solution-processable organic semiconductors, using other semiconducting cores that exhibit denser packing and thus enhanced charge transport in monodomain field-effect transistors.

Acknowledgment. We thank Dr. H. Wondergem of Philips Research for measuring X-ray spectra, Dr. K. Genevicius, Dr. M. Shkunov and Dr. I. McCulloch from Merck Chemicals for assistance with the TOF measurements and generous supply of liquid crystal cells, Prof. P. Strohriegl from the University of Bayreuth for valuable discussions, and the Dutch Ministry of Economic Affairs for supporting this work under the BTS framework program “StableFET”.

Supporting Information Available: Complete ref 2; synthesis and analytical data of compounds **2**−**4**. This material is available free of charge via the Internet at http://pubs.acs.org.

JA055337L

(40) Qiu, Y.; Hu, Y.; Dong, G.; Wang, L.; Xie, J.; Ma, Y. *Appl. Phys. Lett.* **2003**, *83*, 1644.